



# Effective removal of the rare earth element dysprosium from wastewater with polyurethane sponge-supported graphene oxide–titanium phosphate

Peng Xiaoqian<sup>1,2</sup> · Mo Siqi<sup>1</sup> · Li Ruonan<sup>1</sup> · Li Jing<sup>1,2</sup> · Tian Chen<sup>1,2</sup> · Liu Weizhen<sup>1,2</sup> · Wang Yongjing<sup>3</sup>

Received: 26 March 2020 / Accepted: 6 August 2020 / Published online: 18 August 2020  
© Springer Nature Switzerland AG 2020

## Abstract

Recycling methods will be essential for the future circular economy in the context of declining natural resources. Nanomaterials are promising adsorbents to recover rare earth elements from wastewater, yet the practical application of nanomaterials is limited by spontaneous agglomeration, easy collapse of structures and the difficulty in collecting nanomaterials after adsorption. To solve these issues, we prepared a polyurethane sponge-supported titanium phosphate with graphene oxide, abbreviated as GO@TiP-Sponge, by in situ precipitation. GO@TiP-Sponge was characterized by X-ray diffraction, scanning electron microscope, energy-dispersive X-ray spectroscopy and X-ray photoelectron spectroscopy, and tested for the removal and recovery of trace dysprosium Dy(III), a rare-earth element, in water using batch experiments. Results show that the GO@TiP-Sponge showed an excellent affinity for dysprosium with theoretical capacity reaching 576.17 mg/g according to the Langmuir model. Half-equilibrium was reached in 2.5 min according to a pseudo-second-order model. GO@TiP-Sponge also displayed an adsorption ability for a wide range of pH and salinity. Such performance is explained by strong binding of phosphate with Dy(III), enhanced surface area induced by graphene oxide and less aggregation from the spongy structure. The main adsorption mechanism involves electrostatic interaction.

**Keywords** Sponge · Graphene oxide · Titanium phosphate · Composites · Dy(III) · Recovery

**Electronic supplementary material** The online version of this article (<https://doi.org/10.1007/s10311-020-01073-y>) contains supplementary material, which is available to authorized users.

✉ Liu Weizhen  
weizhliu@scut.edu.cn

✉ Wang Yongjing  
yjiang03@fzu.edu.cn

<sup>1</sup> School of Environment and Energy, Guangdong Provincial Key Laboratory of Solid Wastes Pollution Control and Recycling, South China University of Technology, Guangzhou 510006, Guangdong, People's Republic of China

<sup>2</sup> Sino-Singapore International Joint Research Institute (SSIJRI), Guangzhou 510000, Guangdong, People's Republic of China

<sup>3</sup> College of Environment and Resources, Fuzhou University, Fuzhou 350000, Fujian, People's Republic of China

## Introduction

Water contamination is a rising global issue (Basheer 2018; Alharbi et al. 2018). Owing to the continuous exploitation of rare earth, a mass of rare earth elements wastewater was discarded to the environment, which caused serious pollution (Chao et al. 2016). Since the 1990s, the rare earth elements have been listed as major pollutants in China (Liu et al. 2015b). And the rare earth elements were widely used in merging clean energy technologies (Zaimes et al. 2015), national defense applications (Yang et al. 2013), medical application (Hernandez-Adame et al. 2017), due to the unique physical and chemical properties. With the advent of advanced technologies, there is a rising demand for rare earth elements in the global markets (Dutta et al. 2016); however, the rare earth elements resource is facing serious shortage because of their low reserves and outputs from the natural minerals (Li et al. 2018). Therefore, many secondary resources with low concentrations of rare earth elements have attracted extensive attention. The enrichment and recovery of low-concentration rare earth elements on solid

waste have been greatly developed, but the rare earth recovery in the wastewater is an overlooked point (Qin et al. 2019; Qiu et al. 2020). Less than 1% of the rare earth elements used today were actually recycled up (Jowitt et al. 2018), and it is still a challenge for recycling low-concentration rare earth elements.

Adsorption was regarded as an effective technology for treating wastewater due to its high extraction capacity (Ali et al. 2019), inexpensive price (Ali 2018), simple operation (Zhou et al. 2018), wider applicability (Crini et al. 2019), etc. Compared with other adsorbents, nanomaterials exhibit higher surface activity (Peng et al. 2019), higher porosity (Madhura et al. 2019) and more adsorption active sites (Madima et al. 2020), thereby gaining importance of researchers toward their applications in this area (Al-Shaalan et al. 2019; Nodeh et al. 2016). Nanomaterials which have been commonly used for the rare earth elements wastewater include titanium phosphate (Jia et al. 2008), graphene oxide (Ashour et al. 2017), metal–organic framework (MOF) structure materials (Lee et al. 2018), modified mesoporous carbon materials (Koochaki-Mohammadpour et al. 2014), etc. They showed advantages in extracting the rare earth elements of low concentrations. For instance, Zhang et al. recovered trace scandium from leachates of waste bauxite residue by titanium phosphate ion exchangers (Zhang et al. 2017). Li et al. combined titanium phosphate with graphene oxide (recorded as GO@TiP) by in situ precipitation, which showed excellent adsorption capacity for  $\text{Eu}^{3+}$  from acidic solution (Li et al. 2014). However, it is an unavoidable problem that the nanomaterials including titanium phosphate and GO@TiP were spontaneous to agglomerated (Tian et al. 2017) and difficult to be collected and reused (Song et al. 2019), with the structures prone to collapse (Li et al. 2018). Moreover, it was also a possible risk that the release of nanoparticles into the environment impacted plant behavior (Dev et al. 2018) and human health ((Liu et al. 2019; Zhao et al. 2011). These drawbacks limit its application despite the high adsorption capacities.

It was an effective approach for overcoming the above problems by fabricating nanomaterials onto high-mechanical-strength supporting materials (Tesh and Scott 2014; Zhao et al. 2011). The nanoparticle could be successfully uploaded on the supporting material by forming hydrogen bonds or through mechanical forces (Yu et al. 2008). The resultant nanocomposite not only retains the inherent properties of nanomaterials but also keeps the mechanical strength of supporting materials (Chen et al. 2016). The widely used supporting materials contained inorganic materials (Chen et al. 2017), some carbon materials (Li et al. 2018), etc. Polyurethane sponge (PU) was a kind of commercially available 3D porous material with porous structure (Mao et al. 2018), high absorption ability (Zhou et al. 2016), good elasticity, high mechanical durability (Zhu et al. 2013) and low

cost for large-scale production (Liu et al. 2015a, b), which has attracted promising applications in fields of adsorption and separation, etc. It has been reported as a good supporting material for nanoparticles. For example, Zhao et al. (2015) prepared  $\text{TiO}_2$ –graphene sponge for the adsorption of tetracycline antibiotics, which showed higher adsorption capacity than graphene oxide and graphene oxide–chitosan aerogel, meanwhile maintained the high-strength property of the sponge.

In this work, polyurethane sponge-supported titanium phosphate with graphene oxide (recorded as GO@TiP-Sponge) was synthesized by in situ precipitation of graphene oxide, titanium phosphate and sponge. GO@TiP-Sponge was applied to remove and recover the low-concentration Dy(III) from wastewater. Batch experiments showed considerable adsorption ability and fast adsorption rate of GO@TiP-Sponge to Dy(III). Meanwhile, the material can be recycled and showed the high-strength property in the acidic environment. And it is a promising method for the feasible application of GO@TiP-Sponge to remove and recover low-concentration rare earth elements from wastewater.

## Experimental section

### Materials

The detailed information of materials is provided in supporting information.

### Preparation of titanium phosphate, graphene oxide, GO@TiP and GO@TiP-Sponge

Titanium phosphate was synthesized by the same volume of 0.6 mol/L  $\text{H}_3\text{PO}_4$  and 0.3 mol/L  $\text{Ti}(\text{SO}_4)_2$  solution, and synthesis of graphene oxide from graphite powder was carried out by a modified Hummers method (Li et al. 2014). The specific methods are shown in the supporting information.

Sponge samples were cut into uniform blocks of 2 cm × 1 cm × 1 cm in size, and the mass of each block was adjusted to around 80 mg. The sponge was treated ultrasonically with acetone for 1 h, then cleaned with deionized water for 1 h and dried in an oven at 65 °C. The sponge blocks were immersed in 1 mg/mL graphene oxide suspension by 30 min of ultrasonication. Then, with continuous stirring, the same volume of 0.3 mol/L  $\text{Ti}(\text{SO}_4)_2$  and 0.6 mol/L  $\text{H}_3\text{PO}_4$  was added into the suspension containing sponges successively at 65 °C. After aging for 2 h, the wet sponges were freeze-dried for 48 h; then, GO@TiP-Sponge could be obtained. The synthesis process is illustrated in Scheme S1. If we do the same process without putting sponges into the suspension and take the deposit after aging to centrifuge

and dried, we could obtain GO@TiP powder (Li et al. 2014). The loading capacity ( $Q_L$ ) of GO@TiP-Sponge is measured by Eq. 1 as follows:

$$Q_L = \frac{M_1 - M_2}{M_2} \quad (1)$$

where  $Q_L$  is the loading capacity of GO@TiP-Sponge (g/g),  $M_1$  (g) is the mass of synthesis GO@TiP-Sponge and  $M_2$  (g) is the mass of the original sponge.

## Characterization

Detailed information on characterization is given in supporting materials.

## Batch adsorption experiments

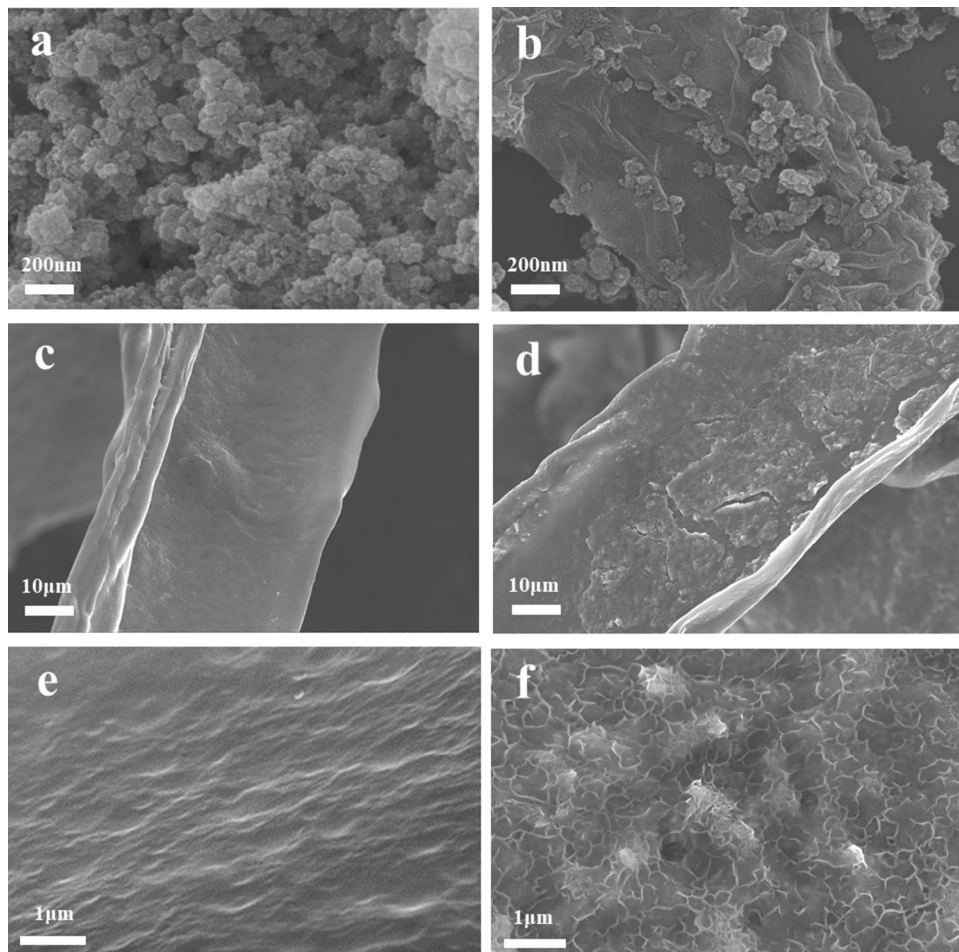
The detailed information of batch adsorption experiments is given in supporting information.

## Results and discussion

### Characterization of the prepared nanomaterials

According to Eq. 1, the loading capacity ( $Q_L$ ) of GO@TiP-Sponge was 0.98 g/g. And Fig S1 shows the X-ray diffraction (XRD) patterns of the prepared nanomaterials including of titanium phosphate, graphene oxide, GO@TiP and GO@TiP-Sponge. A sharp diffraction peak of graphene oxide at  $11.6^\circ$  could be well indexed to the (001) planes of graphene oxide, which confirmed the successful synthesis of graphene oxide (Chen et al. 2013). Titanium phosphate presented no sharp diffraction peaks, only a very broad one at  $20^\circ$ – $30^\circ$ , and the diffraction peaks of titanium phosphate displayed a similar XRD pattern as titanium phosphate in the previous studies, implying that the titanium phosphate particles were amorphous in nature (Jia et al. 2008; Zhang et al. 2017). Meanwhile, the XRD peaks of GO@TiP were close to those of titanium phosphate, suggesting that graphene oxide did not alter the lattice structure of titanium phosphate. However, peaks of graphene oxide were not shown in the XRD

**Fig. 1** Scanning electron microscopy (SEM) images of titanium phosphate (a), GO@TiP (b), clean sponge (c, e), GO@TiP-Sponge (d, f). Note that graphene oxide and titanium phosphate were uniformly loaded on the surface ruffle of the sponge, forming a cascade-crisscross structure. GO@TiP: titanium phosphate combined with graphene oxide; GO@TiP-Sponge: polyurethane sponge-supported graphene oxide with titanium phosphate



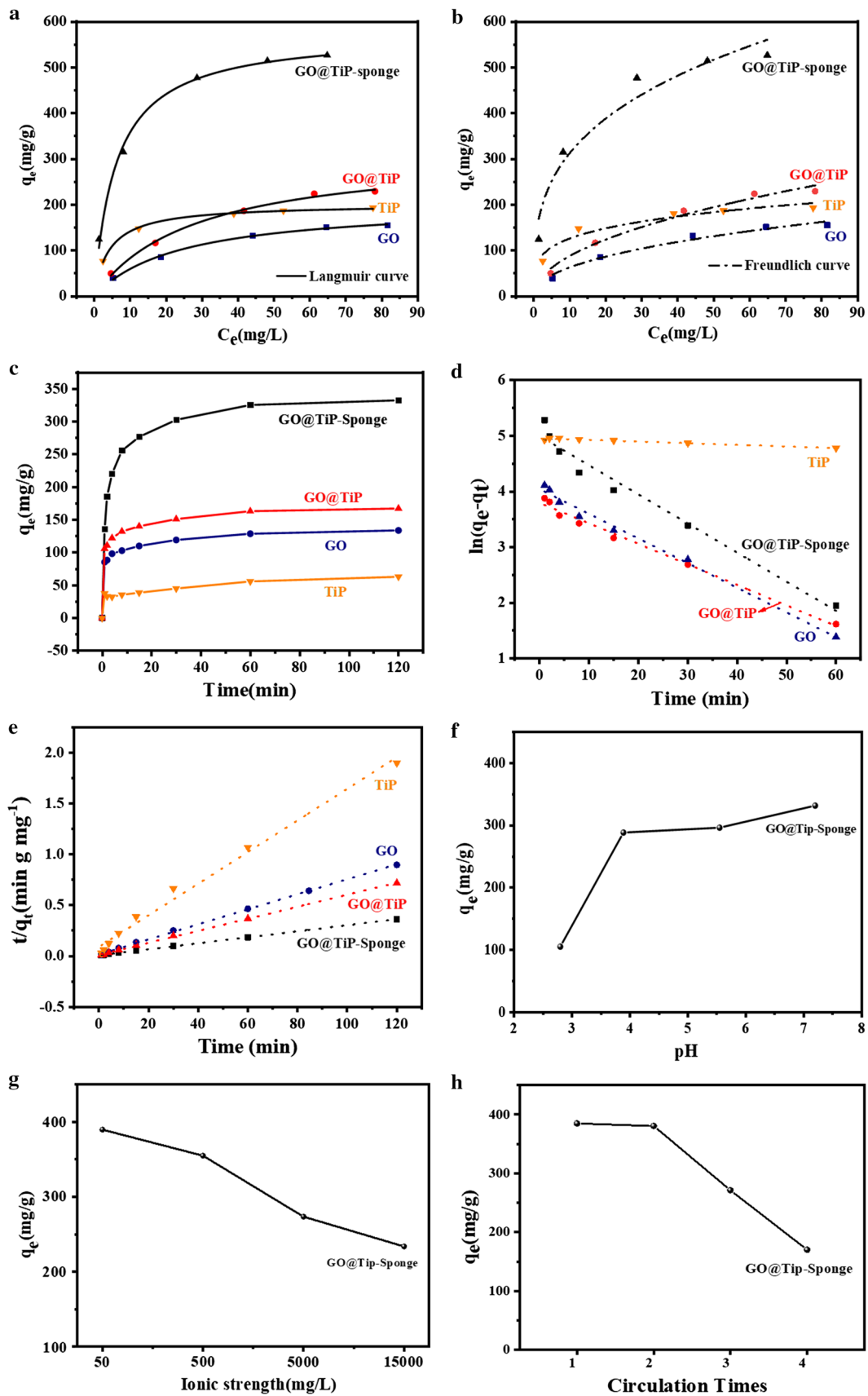


**Fig. 2** Adsorption experiments data: Langmuir (a) and Freundlich (b) isotherms for Dy(III) adsorption by titanium phosphate, graphene oxide, GO@TiP and GO@TiP-Sponge; adsorption kinetics of titanium phosphate, graphene oxide, GO@TiP and GO@TiP-Sponge toward Dy(III) (c); pseudo-first-order kinetic (d) and pseudo-second-order kinetic (e) model fitting for Dy(III) adsorption; the influence of the pH value (f) and the ionic strength (g) on the adsorption capacity of the GO@TiP-Sponge treatment toward Dy(III); the cyclic regeneration experiments of GO@TiP-Sponge adsorbing Dy(III) (h). Ionic strength conditions:  $T=298$  K,  $C_{Dy}=50$  mg/L,  $pH_{\text{sediment}}=7.88$ , the dosage of adsorbent was 0.06 mg/mL. Note that adsorption data obeyed the Langmuir model, the theoretical maximum capacity was 576.17 mg/g and the kinetic adsorption of Dy(III) on these sorbents followed the pseudo-second-order model. The adsorption capacity of GO@TiP-Sponge to Dy(III) stayed high over a wide range of pH and in high ionic strength. The adsorption capacity of GO@TiP-Sponge remained unchanged in the second cycle, and the adsorption capacity was still up to 100 mg/g after 4 cycles. GO: graphic oxide; TiP: titanium phosphate; GO@TiP: titanium phosphate combined with graphene oxide; GO@TiP-Sponge: polyurethane sponge-supported titanium phosphate with graphene oxide

pattern of the GO@TiP and GO@TiP-Sponge. This implied that either all stacking of graphene layers was lost or any remaining stacking was disordered when it was composited with titanium phosphate (McAllister et al. 2007). Moreover, XRD patterns for GO@TiP-Sponge seem to have no relation with GO@TiP, implying that the structure of sponge is dominated in the composite material.

Morphologies of the titanium phosphate, GO@TiP and GO@TiP-Sponge were characterized by scanning electron microscopy (SEM). As shown in Fig. 1a, the native titanium phosphate prone to form irregular aggregates within the size of no more than 100 nm. Compared with titanium phosphate, the aggregation of GO@TiP was largely reduced. It could be observed that smaller titanium phosphate aggregated randomly deposit on the surface of graphene oxide lamellar (Fig. 1b). After the successive uploading of graphene oxide and titanium phosphate on the sponge, the clean and smooth sponge surface changed to a rough structure (Fig. 1c, d). Further observation of the locally enlarged view revealed that the GO@TiP was uniformly loaded on the surface ruffle of the sponge, forming a cascade-crisscross structure (Fig. 1e, f). The primary particles of such a hierarchical structure were lamellae with a thickness of ~tens of nm and a width of ~hundreds of nm. The energy-dispersive X-ray spectroscopy (EDS) analysis of the selected area in the SEM image of GO@TiP-Sponge proved the existence of Ti, C, P and O elements (Fig S2), suggesting the nanolamellae on the sponge surfaces were composed of titanium phosphate. Compared with the native titanium phosphate and GO@TiP, titanium phosphate particles were much more dispersed in the structure of GO@TiP-Sponge, which would be beneficial for the adsorption of the rare earth elements.

The Brunauer–Emmett–Teller (BET) surface areas for titanium phosphate, GO@TiP and GO@TiP-Sponge were

determined to be 150.65 m<sup>2</sup>/g and 173.68 m<sup>2</sup>/g and 1.52 m<sup>2</sup>/g, as shown in Table S1. Since the high surface area of one layer graphene (theoretical value: 2630 m<sup>2</sup>/g) (Ning et al. 2011), the specific surface area of GO@TiP increased than titanium phosphate. On the other hand, the relative higher value of the specific surface area of GO@TiP could be ascribed to the intercalation of titanium phosphate particles onto the graphene oxide sheets, which avoided the aggregation of both graphene oxide and titanium phosphate (Montes-Navajas et al. 2013). However, the surface area of GO@TiP-Sponge was much smaller, because the surface area of the naked polyurethane sponge was extremely low (< 1 m<sup>2</sup>/g) (Lin and Chang 2015). After loading graphene oxide and titanium phosphate on the sponge, the resultant GO@TiP-Sponge exhibited higher surface areas than the polyurethane sponge. The N<sub>2</sub> adsorption–desorption isotherms of titanium phosphate, GO@TiP and GO@TiP-Sponge at 77 K is shown in Fig S3. With a clear hysteresis loop, the type IV isotherm curves indicated that all three materials possess typical mesoporous structures.

## Adsorption experiments

### Adsorption isotherms and kinetics

The Langmuir model gave a higher correlation coefficient ( $R^2 > 0.99$ ) than the Freundlich model and thus was more suitable to describe the adsorption of Dy(III) by four kinds of adsorbents that titanium phosphate, graphene oxide, GO@TiP, GO@TiP-Sponge, indicating that monolayer adsorption was the basic mechanism (Fig. 2a, b). By applying the Langmuir model, the theoretical maximum capacity ( $Q_m$ ) of GO@TiP-Sponge on Dy(III) was 576.17 mg/g (Table S2), which was higher than graphene oxide (203.75 mg/g), titanium phosphate (201.51 mg/g) and GO@TiP (316.75 mg/g). Such excellent adsorption property could be related to the dispersed structure of titanium phosphate on the sponge which permitted more active sites for adsorption.

Adsorption kinetic data showed that those adsorbents could reach equilibrium in 20 min (Fig. 2c). The kinetic adsorption of Dy(III) on these sorbents followed the pseudo-second-order model (Fig. 2d, e and Table S3), which implied that the adsorption was a chemical process that involves valency due to electron sharing. Besides, the  $t_{1/2}$  values of GO@TiP-Sponge on Dy(III) was about 2.5 min (Table S4), indicating the quick removal rate of Dy(III) from solutions.

### Effect of pH and ionic strength on adsorption property of adsorbent

In the reality of industrial production, wastewater containing the rare earth elements is slightly acidic. As shown in Fig. 2f, when pH ranges from 2.8 to 3.9, the adsorption

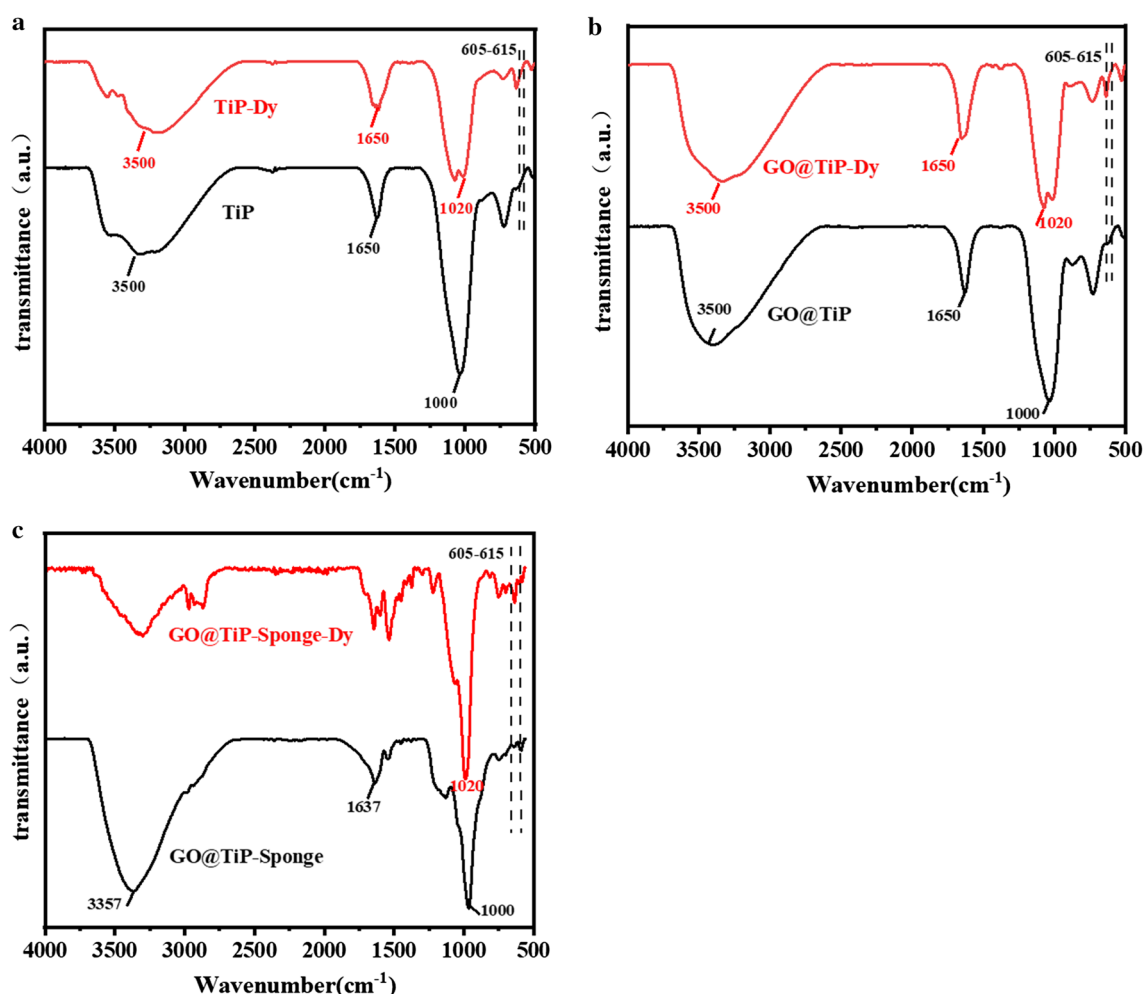


**Fig. 3** Fourier transform infrared (FT-IR) spectroscopy spectra of titanium phosphate (a), GO@TiP (b) and GO@TiP-Sponge (c) before and after adsorption. Note that the shift of the P–OH band from 1000 to 1020  $\text{cm}^{-1}$  was assigned to the electrostatic interactions between the orthophosphate group and Dy(III), implying the interaction mechanism could be regarded as an electrostatic interaction. TiP: titanium phosphate; TiP-Dy: titanium phosphate after adsorbing Dy(III);

GO@TiP: titanium phosphate combined with graphene oxide; GO@TiP-Dy: titanium phosphate combined with graphene oxide after adsorbing Dy(III); GO@TiP-Sponge: polyurethane sponge-supported titanium phosphate with graphene oxide; GO@TiP-Sponge-Dy: polyurethane sponge-supported titanium phosphate with graphene oxide after adsorbing Dy(III)

capacity of Dy(III) by the GO@TiP-Sponge quickly increased with rising pH value. The adsorption capacity for Dy(III) stayed high (288.13 mg/g) over a large range of pH from 3.9 to 5.7, which indicated the effectiveness of these composite adsorbents in the direct uptake of Dy(III) from acidic solutions. The sudden increase in the capacity for Dy(III) when pH change from 6 to 7 may result from the hydrolysis of Dy(III).

There are many other cations in the rare earth elements wastewater. To find out the effect of ionic strength, we introduced NaCl into the adsorption system as a background electrolyte. The adsorption capacity decreased gradually as ionic strength increased (Fig. 2g). However,

even the capacity decreased by 50%, the capacity was still high (203.8 mg/g). This result further supported that this material was practical with its tolerance to high ionic strength. This sensitivity to the change in concentration of the background electrolyte suggests that electrostatic attraction is an important mechanism for Dy(III) adsorption.

### Regeneration and reusability of the adsorbent

The desorption rate of GO@TiP-Sponge is shown in Fig. 2h. The adsorption capacity of GO@TiP-Sponge toward Dy(III) remained unchanged in the second cycle, but started to

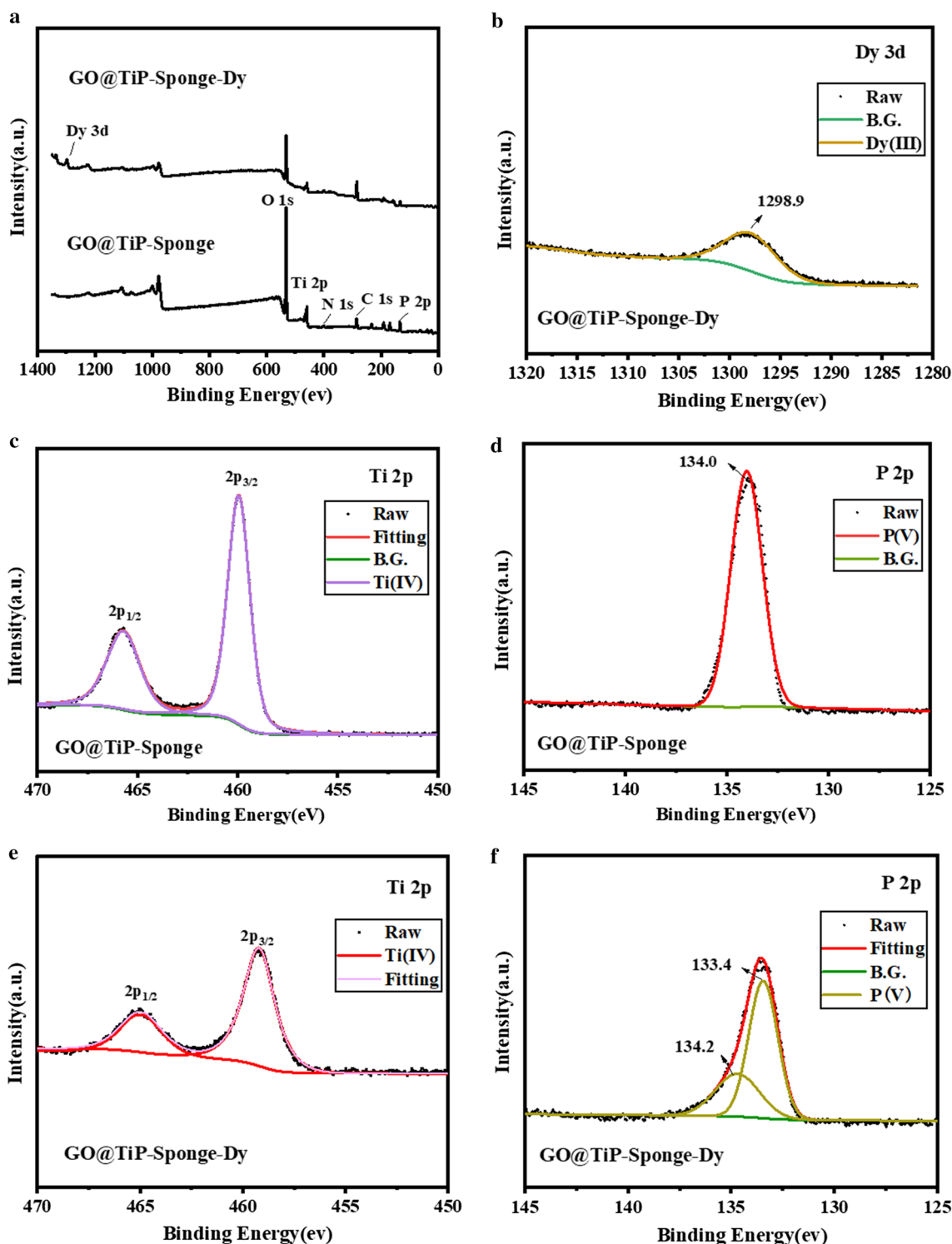


**Fig. 4** a X-ray photoelectron spectroscopy (XPS) survey spectra of GO@TiP-Sponge and GO@TiP-Sponge-Dy. b Dy 3d spectra of GO@TiP-Sponge-Dy. c, d Ti 2p and e, f P 2p spectra of GO@TiP-Sponge before and after the interaction with Dy(III). Note that there were two binding energies of 133.4 eV and 134.2 eV of the high-resolution P 2P region in the GO@TiP-Sponge after adsorbing Dy(III),

which was attributed to  $\text{HPO}_4^{2-}$  or  $\text{PO}_4^{3-}$ . Therefore, the adsorption mechanism could be indicative of electrostatic interactions. GO@TiP-Sponge: polyurethane sponge-supported titanium phosphate with graphene oxide; GO@TiP-Sponge-Dy: polyurethane sponge-supported titanium phosphate with graphene oxide after adsorbing Dy(III)

decrease in the later cycles. Figure S4 shows the SEM images of fresh and regenerated 4 cycles GO@TiP-Sponge. The surface of regenerated GO@TiP-Sponge became more smooth than fresh GO@TiP-Sponge, suggesting that a little of GO@TiP dissolved or detached from the sponge during the process of reusability, which leads to the decrease in the adsorption capacity. Besides, the incomplete desorption of Dy(III) may also lead to a decrease in capacity. Although the adsorption capacity decreased, the regenerated GO@TiP-Sponge still maintained its structure. In general, the adsorption capacity for Dy(III) was still up to 100 mg/g after 4 cycles making regeneration and reuse possible in practical water treatment.

### Adsorption mechanism

Fourier transform infrared (FT-IR) spectroscopy analysis was performed to identify the evolution of the surface functionalities of GO@TiP-Sponge before and after the adsorption of Dy(III). FT-IR showed little changes in the characteristic peaks of adsorbents after Dy(III) adsorption (Fig. 3). As shown in the FT-IR spectra, the presence of external water within titanium phosphate and GO@TiP was confirmed by the sharp peaks at 3500 and 1650  $\text{cm}^{-1}$  (Fig. 3a, b) (Kim et al. 1997; Varshney et al. 1998). And the peak of GO@TiP-Sponge (Fig. 3c) at 1637  $\text{cm}^{-1}$  attributed to the absorbed water or carbonyl groups. OH symmetrical stretching band was observed in the peak at 3357  $\text{cm}^{-1}$  (Hummers Jr and Offeman 1958; Kim et al. 1997; Varshney et al. 1998). The weak band at 605–615  $\text{cm}^{-1}$  meant the deformation vibration for the Ti–O bond (Bortun et al. 1997). The band from 1000 to 1020  $\text{cm}^{-1}$  implied the asymmetric stretching vibration of Ti–P–OH (Kawahara et al. 2000). After uptake of Dy(III), the shift of the P–OH band was assigned to the electrostatic interactions between the orthophosphate group and Dy(III). Therefore, the interaction mechanism could be regarded as an electrostatic interaction.

X-ray photoelectron spectroscopy (XPS) investigated the valance states of the surface atoms for GO@TiP-Sponge after the Dy(III) adsorption. The XPS survey spectrum of GO@TiP-Sponge before and after the adsorption is shown in Fig. 4a. Compared with the GO@TiP-Sponge, the intense peaks of Dy 3d have been introduced by the adsorption process (Fig. 4a). High-resolution Dy 3d XPS peaks were commonly observed at 1298.9 eV (Fig. 4b), which revealed that Dy existed in a trivalent state (Kang et al. 2015; Padalia et al. 1977) and there was no redox reaction in the adsorption process. The curve-fitted Ti 2p spectra of the GO@TiP-Sponge and GO@TiP-Sponge after adsorbing Dy(III) (recorded as GO@

TiP-Sponge-Dy) are given in Fig. 4c, e. It can be seen that the Ti 2p distinct peaks of GO@TiP-Sponge-Dy were found at similar positions with the primary GO@TiP-Sponge corresponding to the binding energy of 459.25 eV and 465.48 eV. It was attributed to Ti 2p<sub>3/2</sub> and Ti 2p<sub>1/2</sub>, respectively, which implied that Ti existed in a tetravalent state (Moulder et al. 1992). For GO@TiP-Sponge, the experimentally obtained XPS P 2p peak binding energy of 134.0 eV (Fig. 4d) agreed with values obtained for P(V) in oxide (Barboux et al. 1992). It was in good agreement with the elemental atomic ratio shown in Fig S2. Besides, after peak deconvolution of the high-resolution P 2P region (Fig. 4f), there were two contributions (133.4 and 134.2 eV) in the GO@TiP-Sponge after adsorbing Dy(III), which exhibited differences with that in the primary GO@TiP-Sponge. The binding energy of 133.4 eV and 134.2 eV was attributed to  $\text{HPO}_4^{2-}$  or  $\text{PO}_4^{3-}$  (Barboux et al. 1992; Lo et al. 1994), which was assigned to combined with Dy(III); thus, the adsorption mechanism could be indicative of electrostatic interactions. The conclusion is similar to the FT-IR analysis.

### Conclusion

In summary, an efficient adsorption material has been successfully synthesized by the co-precipitation method and was characterized by XRD, SEM, BET, FT-IR and XPS. GO@TiP-Sponge combined the advantage of graphene oxide and titanium phosphate, which led to high absorption ability and brilliant recycling potential. The measured isotherms showed that the Langmuir model simulated the process well with  $Q_m$  of 576.17 mg/g for Dy(III). The half-equilibrium time of this material was 2.5 min, and this material was practical with its tolerance to high ionic strength. Meanwhile, it also shows considerable adsorption ability in a wide range of pH, leading to great application values in the industry. FT-IR and XPS results suggested that the adsorption mechanism was electrostatic interactions between  $\text{PO}_4^{3-}$  and Dy(III). This work provides an effective strategy by utilizing the promising adsorption material of GO@TiP-Sponge for the rare earth elements wastewater treatment.

**Acknowledgements** The authors would like to express thanks to the support by the National Key Research and Development Program of China (No. 2019YFA0210400), the Guangdong Innovative and Entrepreneurial Research Team Program (No. 2016ZT06N569), the Guangdong Science and Technology Program (No. 2020B121201003), the Scientific and Technical Innovative Youth Talents of Guangdong Special Support Program (No. 2019TQ05L153) and the Guangzhou Science and Technology Project (No. 201804010189).



## References

- Alharbi OM, Khattab RA, Ali I (2018) Health and environmental effects of persistent organic pollutants. *J Mol Liq* 263:442–453. <https://doi.org/10.1016/j.molliq.2018.05.029>
- Ali I (2018) Microwave assisted economic synthesis of multi walled carbon nanotubes for arsenic species removal in water: batch and column operations. *J Mol Liq* 271:677–685. <https://doi.org/10.1016/j.molliq.2018.09.021f>
- Ali I, Alharbi OM, Al Othman ZA, Al-Mohaimed AM, Alwarthan A (2019) Modeling of fenuron pesticide adsorption on CNTs for mechanistic insight and removal in water. *Environ Res* 170:389–397. <https://doi.org/10.1016/j.envres.2018.12.066>
- Al-Shaalan NH, Ali I, Al Othman ZA, Al-Wahaibi LH, Alabdulmonem H (2019) High performance removal and simulation studies of diuron pesticide in water on MWCNTs. *J Mol Liq* 289:111039. <https://doi.org/10.1016/j.molliq.2019.11.1039>
- Ashour RM et al (2017) Rare earth ions adsorption onto graphene oxide nanosheets. *Solvent Extr Ion Exc* 35:91–103. <https://doi.org/10.1080/07366299.2017.1287509>
- Barboux Y, Dekiouk M, Le Maguer D, Gengembre L, Huchette D, Grimblot J (1992) Bulk and surface analysis of a Fe-PO oxydehydrogenation catalyst. *Appl Catal A* 90:51–60. [https://doi.org/10.1016/0926-860X\(92\)80247-A](https://doi.org/10.1016/0926-860X(92)80247-A)
- Basheer AA (2018) New generation nano-adsorbents for the removal of emerging contaminants in water. *J Mol Liq* 261:583–593. <https://doi.org/10.1016/j.molliq.2018.04.021>
- Bortun AI, Khainakov SA, Bortun LN, Poojary DM, Rodriguez J, Garcia JR, Clearfield A (1997) Synthesis and characterization of two novel fibrous titanium phosphates  $Ti_2O(PO_4)_2 \cdot 2H_2O$ . *Chem Mater* 9:1805–1811. <https://doi.org/10.1021/cm970060c>
- Chao YQ et al (2016) Structure, variation, and co-occurrence of soil microbial communities in abandoned sites of a rare earth elements mine. *Environ Sci Technol* 50:11481–11490. <https://doi.org/10.1021/acs.est.6b02284>
- Chen FJ, Cao YL, Jia DZ (2013) A room-temperature solid-state route for the synthesis of graphene oxide–metal sulfide composites with excellent photocatalytic activity. *CrystEngComm* 15:4747–4754. <https://doi.org/10.1039/C3CE40079D>
- Chen D et al (2016) Micro–nanocomposites in environmental management. *Adv Mater* 28:10443–10458. <https://doi.org/10.1002/adma.201601486>
- Chen M et al (2017) FeOOH-loaded  $MnO_2$  nano-composite: an efficient emergency material for thallium pollution incident. *J Environ Manage* 192:31–38. <https://doi.org/10.1016/j.jenvman.2017.01.038>
- Crini G, Lichtfouse E, Wilson LD, Morin-Crini N (2019) Conventional and non-conventional adsorbents for wastewater treatment. *Environ Chem Lett* 17:195–213. <https://doi.org/10.1007/s10311-018-0786-8>
- Dev A, Srivastava AK, Karmakar S (2018) Nanomaterial toxicity for plants. *Environ Chem Lett* 16:85–100. <https://doi.org/10.1007/s10311-017-0667-6>
- Dutta T, Kim KH, Uchimiya M, Kwon EE, Jeon BH, Deep A, Yun ST (2016) Global demand for rare earth resources and strategies for green mining. *Environ Res* 150:182–190. <https://doi.org/10.1016/j.envres.2016.05.052>
- Hernandez-Adame L et al (2017) Toxicity evaluation of high-fluorescent rare-earth metal nanoparticles for bioimaging applications. *J Biomed Mater Res B Appl Biomater* 105:605–615. <https://doi.org/10.1002/jbm.b.33577>
- Hummers WS Jr, Offeman RE (1958) Preparation of graphitic oxide. *J Am Chem Soc* 80:1339–1339. <https://doi.org/10.1021/ja01539a017>
- Jia K et al (2008) Adsorption of  $Pb^{2+}$ ,  $Zn^{2+}$ , and  $Cd^{2+}$  from waters by amorphous titanium phosphate. *J Colloid Interf Sci* 318:160–166. <https://doi.org/10.1016/j.jcis.2007.10.043>
- Jowitt SM, Werner TT, Weng Z, Mudd GM (2018) Recycling of the rare earth elements. *Curr Opin Green Sustain Chem* 13:1–7. <https://doi.org/10.1016/j.cogsc.2018.02.008>
- Kang JG, Gwag JS, Sohn Y (2015) Synthesis and characterization of  $Dy(OH)_3$  and  $Dy_2O_3$  nanorods and nanosheets. *Ceram Int* 41:3999–4006. <https://doi.org/10.1016/j.ceramint.2014.11.085>
- Kawahara M, Morita J, Rikukawa M, Sanui K, Ogata N (2000) Synthesis and proton conductivity of thermally stable polymer electrolyte: poly(benzimidazole) complexes with strong acid molecules. *Electrochim Acta* 45:1395–1398. [https://doi.org/10.1016/S0013-4686\(99\)00349-7](https://doi.org/10.1016/S0013-4686(99)00349-7)
- Kim HN, Keller SW, Mallouk TE, Schmitt J, Decher G (1997) Characterization of zirconium phosphate/polycation thin films grown by sequential adsorption reactions. *Chem Mater* 9:1414–1421. <https://doi.org/10.1021/cm970027q>
- Koochaki-Mohammadpour SMA, Torab-Mostaedi M, Talebizadeh-Rafsanjani A, Naderi-Behdani F (2014) Adsorption isotherm, kinetic, thermodynamic, and desorption studies of lanthanum and dysprosium on oxidized multiwalled carbon nanotubes. *J Dispers Sci Technol* 35:244–254. <https://doi.org/10.1080/01932691.2013.785361>
- Lee Y, Yu K, Ravi S, Ahn W (2018) Selective adsorption of rare earth elements over functionalized Cr-MIL-101. *ACS Appl Mater Inter* 10:23918–23927. <https://doi.org/10.1021/acsami.8b07130>
- Li C, Huang Y, Lin Z (2014) Fabrication of titanium phosphate@graphene oxide nanocomposite and its super performance on  $Eu^{3+}$  recycling. *J Mater Chem A* 2:14979–14985. <https://doi.org/10.1039/C4TA02983F>
- Li Y, Tian C, Liu W, Xu S, Xu Y, Cui R, Lin Z (2018) Carbon cloth supported nano- $Mg(OH)_2$  for the enrichment and recovery of rare earth element Eu(III) from aqueous solution. *Front Chem* 6:118. <https://doi.org/10.3389/fchem.2018.00118>
- Lin KA, Chang HA (2015) A zeolitic imidazole framework (ZIF)–sponge composite prepared via a surfactant-assisted dip-coating method. *J Mater Chem A* 3:20060–20064. <https://doi.org/10.1039/C5TA04427H>
- Liu S, Xu Q, Lathe SS, Gurav AB, Xing R (2015a) Superhydrophobic/superoleophilic magnetic polyurethane sponge for oil/water separation. *RSC Adv* 5:68293–68298. <https://doi.org/10.1039/C5RA12301A>
- Liu WS, Liu C, Wang ZW, Teng WK, Tang YT, Qiu RL (2015b) Limiting factors for restoration of dumping sites of ionic rare earth mine tailings. *Acta Pedofol Sin* 52:179–187
- Liu W, Weng C, Zheng J, Peng X, Zhang J, Lin Z (2019) Emerging investigator series: treatment and recycling of heavy metals from nanoslug. *Environ Sci Nano* 6:1657–1673. <https://doi.org/10.1039/C9EN00120D>
- Lo PH, Tsai WT, Lee JT, Hung MP (1994) Role of phosphorus in the electrochemical behavior of electroless Ni–P alloys in 3.5 wt.% NaCl solutions. *Surf Coat Technol* 67:27–34. [https://doi.org/10.1016/S0257-8972\(05\)80023-4](https://doi.org/10.1016/S0257-8972(05)80023-4)
- Madhura L, Singh S, Kanchi S, Sabela M, Bisetty K (2019) Nanotechnology-based water quality management for wastewater treatment. *Environ Chem Lett* 17:65–121. <https://doi.org/10.1007/s10311-018-0778-8>
- Madima N, Mishra SB, Inamuddin I, Mishra AK (2020) Carbon-based nanomaterials for remediation of organic and inorganic pollutants from wastewater. A review. *Environ Chem Lett* 18:1169–1191. <https://doi.org/10.1007/s10311-020-01001-0>
- Mao X, Wang L, Wang C, Lichtfouse E (2018) Glutathione-functionalized melamine sponge, a mimic of a natural antidote, as a quick responsive adsorbent for efficient removal of Hg(II) from

- aqueous solutions. *Environ Chem Lett* 16:1429–1434. <https://doi.org/10.1007/s10311-018-0746-3>
- McAllister MJ et al (2007) Single sheet functionalized graphene by oxidation and thermal expansion of graphite. *Chem Mater* 19:4396–4404. <https://doi.org/10.1021/cm0630800>
- Montes-Navajas P, Asenjo NG, Santamaría R, Menendez R, Corma A, García H (2013) Surface area measurement of graphene oxide in aqueous solutions. *Langmuir* 29:13443–13448. <https://doi.org/10.1021/la4029904>
- Moulder JF, Stickle WF, Sobol PE, Bomben KD (1992) Handbook of X-Ray photoelectron spectroscopy, physical electronics division, Perkin Elmer Corp, Eden Prairie, MN
- Ning G, Fan Z, Wang G, Gao J, Qian W, Wei F (2011) Gram-scale synthesis of nanomesh graphene with high surface area and its application in supercapacitor electrodes. *Chem Commun* 47:5976–5978. <https://doi.org/10.1039/C1CC11159K>
- Nodeh HR, Ibrahim WAW, Ali I, Sanagi MM (2016) Development of magnetic graphene oxide adsorbent for the removal and pre-concentration of As(III) and As(V) species from environmental water samples. *Environ Sci Pollut Res* 23:9759–9773. <https://doi.org/10.1007/s11356-016-6137-z>
- Padalia BD, Lang WC, Norris PR, Watson LM, Fabian DJ (1977) X-ray photoelectron core-level studies of the heavy rare-earth metals and their oxides. *Proc R Soc Lond A* 354:269–290. <https://doi.org/10.1098/rspa.1977.0067>
- Peng M et al (2019) PCN-224/rGO nanocomposite based photoelectrochemical sensor with intrinsic recognition ability for efficient p-arsanilic acid detection. *Environ Sci Nano* 6:207–215. <https://doi.org/10.1039/C8EN00913A>
- Qin B et al (2019) Vacuum pyrolysis method for reclamation of rare earth elements from hyperaccumulator *Dicranopteris dichotoma* grown in contaminated soil. *J Clean Prod* 229:480–488. <https://doi.org/10.1016/j.jclepro.2019.05.031>
- Qiu R et al (2020) Recovering full metallic resources from waste printed circuit boards: a refined review. *J Clean Prod* 244:118690. <https://doi.org/10.1016/j.jclepro.2019.118690>
- Song Y, Li J, Li Y, Xu Y, Tian C, Weng C, Liu W (2019) Enrichment and recovery of low-concentration REEs from water using synthesized eco-friendly sodium alginate/nano-Mg(OH)<sub>2</sub> composite beads. *Surf Interfaces* 15:232–238. <https://doi.org/10.1016/j.surfin.2019.03.004>
- Tesh SJ, Scott TB (2014) Nano-composites for water remediation: a review. *Adv Mater* 26:6056–6068. <https://doi.org/10.1002/adma.201401376>
- Tian C, Zhao J, Zhang J, Chu S, Dang Z, Lin Z, Xing B (2017) Enhanced removal of roxarsone by Fe<sub>3</sub>O<sub>4</sub>@3D graphene nanocomposites: synergistic adsorption and mechanism. *Environ Sci Nano* 4:2134–2143. <https://doi.org/10.1039/C7EN00758B>
- Varshney KG, Pandith AH, Gupta U (1998) Synthesis and characterization of zirconium aluminophosphate. A new cation exchanger. *Langmuir* 14:7353–7358. <https://doi.org/10.1021/la970464j>
- Yang XJ, Lin A, Li X, Wu Y, Zhou W, Chen Z (2013) China's ion-adsorption rare earth resources, mining consequences and preservation. *Environ Dev* 8:131–136. <https://doi.org/10.1016/j.envdev.2013.03.006>
- Yu Q, Wu P, Xu P, Li L, Liu T, Zhao L (2008) Synthesis of cellulose/titanium dioxide hybrids in supercritical carbon dioxide. *Green Chem* 10:1061–1067. <https://doi.org/10.1039/B806094K>
- Zaimes GG, Hubler BJ, Wang S, Khanna V (2015) Environmental life cycle perspective on rare earth oxide production. *ACS Sustain Chem Eng* 3:237–244. <https://doi.org/10.1021/sc500573b>
- Zhang W, Koivula R, Wiikinkoski E, Xu J, Hietala S, Lehto J, Harjula R (2017) Efficient and selective recovery of trace scandium by inorganic titanium phosphate ion-exchangers from leachates of waste bauxite residue. *ACS Sustain Chem Eng* 5:3103–3114. <https://doi.org/10.1021/acssuschemeng.6b02870>
- Zhao X, Lv L, Pan B, Zhang W, Zhang S, Zhang Q (2011) Polymer-supported nanocomposites for environmental application: a review. *Chem Eng J* 170:381–394. <https://doi.org/10.1016/j.cej.2011.02.071>
- Zhao L et al (2015) TiO<sub>2</sub>-graphene sponge for the removal of tetracycline. *J Nanopart Res* 17:16. <https://doi.org/10.1007/s11051-014-2825-0>
- Zhou S, Hao G, Zhou X, Jiang W, Wang T, Zhang N, Yu L (2016) One-pot synthesis of robust superhydrophobic, functionalized graphene/polyurethane sponge for effective continuous oil–water separation. *Chem Eng J* 302:155–162. <https://doi.org/10.1016/j.cej.2016.05.051>
- Zhou X, Liu W, Tian C, Mo S, Liu X, Deng H, Lin Z (2018) Mussel-inspired functionalization of biological calcium carbonate for improving Eu(III) adsorption and the related mechanisms. *Chem Eng J* 351:816–824. <https://doi.org/10.1016/j.cej.2018.06.142>
- Zhu Q, Chu Y, Wang Z, Chen N, Lin L, Liu F, Pan Q (2013) Robust superhydrophobic polyurethane sponge as a highly reusable oil-adsorption material. *J Mater Chem A* 1:5386–5393. <https://doi.org/10.1039/C3TA00125C>

**Publisher's Note** Springer Nature remains neutral with regard to jurisdictional claims in published maps and institutional affiliations.